

Modified embedded-atom potentials for cubic materials and impurities

M. I. Baskes

Materials and Process Research Department, Sandia National Laboratories, Livermore, California 94551-0969

(Received 4 November 1991)

In a comprehensive study, the modified embedded-atom method is extended to a variety of cubic materials and impurities. In this extension, all functions are analytic and computationally simple. The basic equations of the method are developed and applied to 26 elements: ten fcc, ten bcc, three diamond cubic, and three gaseous materials. The materials modeled include metals, semiconductors, and diatomic gases, all of which exhibit different types of bonding. Properties of these materials, including equation of state, elastic moduli, structural energies and lattice constants, simple defects, and surfaces, are calculated. The formalism for applying the method to combinations of these elements is developed and applied to the calculation of dilute heats of solution. In all cases, comparison is made to experiment or higher-level calculations when possible.

I. INTRODUCTION

In the past few years the methods for empirical and semiempirical calculations of metals and covalent materials have evolved rapidly. These methods have recently been reviewed by Carlsson,¹ in an MRS Symposium,² and at a special symposium of the World Materials Congress.³ A brief summary of the most closely related work is included here. The embedded-atom method (EAM) of Daw and Baskes,^{4,5} which is based on density-functional theory, has been successfully applied to the fcc or nearly filled *d*-band transition metals. The EAM has also been applied to bcc metals.^{6,7} A number of recent papers summarize the technique and its many applications.⁸⁻¹⁵ Finnis and Sinclair¹⁶ derived the *N*-body potential method based on a second-moment approximation to tight binding and originally applied it to the bcc or half-filled *d*-band transition metals. Rosato, Guillope, and Legrand¹⁷ developed a similar method for the fcc transition metals. An analytic nearest-neighbor model of the EAM for fcc materials was developed by Johnson.¹⁸ This model had the limitation that all materials were forced to have the same anisotropy ratio. Smith and Banerjee¹⁹ developed the equivalent-crystal model and Ercolessi, Tosatti, and Parrinello²⁰ another model, both of which are mathematically equivalent to the EAM. Baskes²¹ modified the EAM to include directional bonding and applied it to silicon. This paper contains references to the many other three-body potentials that have been used to describe the directional bonding in silicon. Brenner²² used the analytic form of one of these silicon potentials²³ to model the carbon, oxygen, and hydrogen systems. The silicon EAM model was extended by Baskes, Nelson, and Wright²⁴ to the silicon-germanium system where the modified embedded-atom method (MEAM) was developed. In the initial version of the MEAM a number of deficiencies were identified: inward relaxation at a vacancy, an extremely large stacking fault energy, and only qualitatively accurate small cluster predictions. Recent calculations²⁵ have shown that the relaxation at a

vacancy should be inward. The partial resolution of the other deficiencies will be discussed below, but, in general, the method presented here is close enough to the original MEAM that the solution of these problems is not expected. Savino, Rao, and Pasianot²⁶ developed a related method based on second-order invariants. All of these methods are mathematically similar and have in common the attribute that the interaction between two atoms depends upon their local environment. It is mainly this fact that accounts for the huge successes that these methods have had in predicting effects at metallic surfaces where the atomic environment is significantly different from the bulk.

It is the objective of this manuscript to extend the MEAM and apply it to a large number of elements to show its wide range of applicability. Our extension is empirical and has *not* been justified by strong physical arguments as have the EAM and *N*-body potential methods. It is not our purpose at this point to obtain optimum potentials for all of the materials considered, but rather to set up a framework that may be used for atomistic calculations. An underlying theme in the development of the method is computational simplicity so that the interactions may be readily used for large molecular dynamics or Monte Carlo simulations. The reader is warned that the potentials presented here require further verification before detailed calculations are performed.

Not only will the MEAM be applied to metals and semiconductors, but we will develop the method so that it is applicable to diatomic gaseous elements. In the process of extending these methods, it was found that a simplification to first-neighbor interactions for all crystal structures (including bcc and hcp) was possible. In addition, a simple analytical model of the embedding function was found to be sufficient to mimic the basic properties of all of the elements considered. In Sec. II, the model is developed and the resultant analytic equations for the elastic constants and simple defects are given. Section III includes the application of the model to surfaces and metastable structures. Section IV includes a discussion of

the application to binary systems and Sec. V is a summary.

II. THEORY

A. Basic equations

The total energy E of a system of atoms in the embedded-atom method has been shown^{4,5,9,12,27} to be given by an approximation of the form

$$E = \sum_i \left[F_i(\bar{\rho}_i) + \frac{1}{2} \sum_{j (\neq i)} \phi_{ij}(R_{ij}) \right], \quad (1)$$

where the sums are over the atoms i and j . [Throughout the manuscript the subscripts (i, j, k) denote either an atom at a particular site or the type of that atom.] In this approximation, the embedding function F_i is the energy to embed an atom of type i into the background electron density at site i , $\bar{\rho}_i$, and ϕ_{ij} is a pair interaction between atoms i and j whose separation is given by R_{ij} . In the initial formulation of the EAM,^{4,5,27} ϕ was assumed to be entirely repulsive, but it has been shown in the more recent formulations,^{12,28} that the nonuniqueness between ϕ and F allows more general forms for ϕ . In the EAM, $\bar{\rho}_i$ is given by a linear superposition of spherically averaged atomic electron densities, while in the modified embedded-atom method, $\bar{\rho}_i$ is augmented by an angularly dependent term.^{21,24} Let us denote the term in parenthesis in Eq. (1), i.e., the direct contribution to the energy from the i th atom, as E_i . Of course, atom i also indirectly contributes to total energy through its interactions with its neighbors. Then E_i may be written as follows:

$$E_i = F_i(\bar{\rho}_i/Z_i) + \frac{1}{2} \sum_{j (\neq i)} \phi_{ij}(R_{ij}), \quad (2)$$

where, for simplification, we have renormalized the background density by the number of nearest neighbors Z_i in what we call the reference structure of a type- i atom. This renormalization has no real physical consequences; it simply redefines a new embedding function. The reference structure is a crystal structure for which we have detailed information about the behavior of atom i . It is usually, but not necessarily, the equilibrium crystal structure of type- i atoms.

We now follow a similar procedure to that used by Baskes, Nelson, and Wright.²⁴ Consider the case of a homogeneous monatomic solid with interactions limited to first neighbors only. By limiting the interactions to first neighbors only, we introduce a number of important questions about cutoffs or screening. These questions are addressed in the Appendix. In this reference structure for an atom of type i we have

$$E_i^u(R) = F_i(\bar{\rho}_i^0(R)/Z_i) + \frac{Z_i}{2} \phi_{ii}(R), \quad (3)$$

where $\bar{\rho}_i^0(R)$ is the background electron density for the reference structure of atom i and R is the nearest-neighbor distance. Here $E_i^u(R)$ is the energy per atom of the reference structure as a function of nearest-neighbor distance. We will discuss this function in more detail in

the following section. Assuming that $E_i^u(R)$ is known, we may use Eq. (3) to determine the pair interaction for type- i atoms:

$$\phi_{ii}(R) = \frac{2}{Z_i} \{ E_i^u(R) - F_i(\bar{\rho}_i^0(R)/Z_i) \}. \quad (4)$$

Using this definition of the pair interaction, we obtain an alternative to Eq. (2) for the monatomic system. The energy contribution E_i for any configuration of atoms is given by

$$E_i = \frac{1}{Z_i} \sum_{j (\neq i)} E_i^u(R_{ij}) + \left[F_i(\bar{\rho}_i/Z_i) - \frac{1}{Z_i} \sum_{j (\neq i)} F_i(\bar{\rho}_i^0(R_{ij})/Z_i) \right]. \quad (5)$$

This equation has an appealing physical interpretation. The first term in Eq. (5) is simply the average of the energy per atom of the reference lattice at each of the nearest-neighbor distances. Note the similarity between this term and the equivalent crystal model.²⁹

The second term is formed by the difference between the embedding energy at the background electron density actually seen by atom i and the average embedding energy of this atom in the reference lattice at each of the nearest-neighbor distances. In essence we may consider this term a new kind of embedding energy where our embedding reference state is that of the reference lattice rather than isolated atoms.

Using Eq. (5), it is a simple matter to write down expressions for the unrelaxed vacancy formation energy E_v^f and the unrelaxed surface or stacking fault energies $E_{(x)}^f$ in the reference lattice:

$$E_v^f = E_i^0 + Z_i F_i(\bar{\rho}_i^v/Z_i) - Z_d F_i(\bar{\rho}_i^0/Z_i), \quad (6)$$

$$E_{(x)}^f = \sum \left[E_i^0 \frac{Z_i - Z_d}{Z_i} + F_i(\bar{\rho}_i^x/Z_i) - \frac{Z_d}{Z_i} F_i(\bar{\rho}_i^0/Z_i) \right] / A_{(x)}, \quad (7)$$

where E_i^0 is the negative of the minimum energy of the reference lattice (sublimation energy), $\bar{\rho}_i^x$ is the background density at site i , a nearest neighbor to the defect (vacancy, surface, or stacking fault), $A_{(x)}$ is the area per atom of the planar defect, and Z_d is the number of neighbors to site i . Values for Z_d and $A_{(x)}$ are given in Table I. Since for some planar defects there is more than one type of site i , a sum over the different environments (planes) in Eq. (7) is indicated.

So far we have been quite general in our discussion, but to show the applicability of the method, it is necessary to specifically define how to calculate the background density. As mentioned above, the EAM used a linear superposition of spherically averaged atomic electron densities. Previously Daw¹² has shown that the EAM may be improved by adding gradient and higher-order corrections to this simple background density. It is not clear that this approach can be extended to mimic the effects of covalency. We use the original EAM formulation as the

dominant contribution to a series of partial background electron densities. Thus, the first partial background electron density at site i is defined by an equation of the form

$$\rho_i^{(0)} = \sum_{j (\neq i)} \rho_j^{a(0)}(R_{ij}), \quad (8a)$$

where $\rho_j^{a(0)}(R_{ij})$ represents the atomic electron density of a type- j atom at a distance R_{ij} from site i . We generalize this expression by defining a series of correction electron densities that explicitly depend upon the relative positions of neighbors of atom i :

$$(\rho_i^{(1)})^2 = \sum_{\alpha} \left[\sum_{j (\neq i)} x_{ij}^{\alpha} \rho_j^{a(1)}(R_{ij}) \right]^2, \quad (8b)$$

$$\begin{aligned} (\rho_i^{(2)})^2 = & \sum_{\alpha, \beta} \left[\sum_{j (\neq i)} x_{ij}^{\alpha} x_{ij}^{\beta} \rho_j^{a(2)}(R_{ij}) \right]^2 \\ & - \frac{1}{3} \left[\sum_{j (\neq i)} \rho_j^{a(2)}(R_{ij}) \right]^2, \end{aligned} \quad (8c)$$

$$(\rho_i^{(3)})^2 = \sum_{\alpha, \beta, \gamma} \left[\sum_{j (\neq i)} x_{ij}^{\alpha} x_{ij}^{\beta} x_{ij}^{\gamma} \rho_j^{a(3)}(R_{ij}) \right]^2, \quad (8d)$$

where $x_{ij}^{\alpha} = R_{ij}^{\alpha} / R_{ij}$, and R_{ij}^{α} is the α component of the distance vector between atoms j and i . The specific forms for Eqs. (8b)–(8d) are chosen so that the partial background electron densities are invariant to lattice transla-

tion and rotation, scale simply with atomic electron density for homogeneous deformation, and equal zero for a cubic lattice with a center of symmetry. It has been shown previously²⁴ that Eqs. (8b) and (8c) are equivalent to a three-body cos and cos² dependence, respectively. Similarly, Eq. (8d) corresponds to a cos³ dependence. For example, Eq. (8b) may be alternatively written

$$(\rho_i^{(1)})^2 = \sum_{j, k (\neq i)} \rho_j^{a(1)}(R_{ij}) \rho_k^{a(1)}(R_{ik}) \cos(\theta_{jik}),$$

where θ_{jik} is the angle between atoms j , i , and k . In this summation the pairwise term for $j = k$ is included. Note that, for generality, a different atomic electron density is used for each component of the partial background electron density. Because of the geometric way that the densities $\rho_i^{(l)}$ are defined, we may consider that they are related to specific angular momentum contributions (*spdf*) to the background electron density and that the associated atomic electron densities are related to averages of the actual angular momentum dependent atomic electron densities. It is not at all clear what the specific relationships are.

We need to combine the partial background densities to form the total density that is to be used as the argument of the embedding energy. In the spirit of density-functional theory, this one, scalar number needs to represent the electron density throughout all space. At this time there is no clearcut guidance from theory on how we should proceed. At first thought a linear superposition of partial densities seems an obvious choice, but because of the square root introduced by solving for $\rho_i^{(l)}$, $l = 1-3$, a singularity is introduced into the density (and thereby the energy) derivatives. It is possible to avoid this singularity by combining the squares of the densities. Thus, using the simplest dimensional analysis we form the total background density by taking a weighted sum of the squares of the partial background densities:

$$(\bar{\rho}_i)^2 = \sum_{l=0}^3 t_i^{(l)} (\rho_i^{(l)})^2, \quad (9)$$

with weighting functions $t_i^{(l)}$. Without loss of generality we take $t_i^{(0)}$ to be equal to unity. We may think of Eq. (9) as a perturbative expansion of the background density away from the linear superposition $\rho_i^{(0)}$:

$$\bar{\rho}_i = \rho_i^{(0)} \left[1 + \frac{1}{2} \sum_{l=1}^3 t_i^{(l)} (\rho_i^{(l)} / \rho_i^{(0)})^2 + \dots \right]. \quad (9a)$$

The correction terms $l = 1-3$ may be physically thought of as adjustments to the spherical density due to the existence of gradients or divergences or the loss of inversion symmetry respectively. We use Eq. (9) in the calculations presented below, but almost identical results are obtained if the expansion Eq. (9a) is used.

We may easily perform the sum over atoms in Eq. (8) for simplified geometries. In this case, since all $R_{ij} = R$, the nearest-neighbor distance, the atomic density factors out of the sum. Without loss of generality we take the atomic electron density at the equilibrium lattice constant to be unity. Using Eq. (9), the background densities for the reference lattice $\bar{\rho}_i^0$ used in Eqs. (3)–(7) and the de-

TABLE I. Values of the geometry factors $S_i^{(l),x}$ for the perfect lattice ($x=0$), vacancy ($x=v$), high index surfaces [$x=(ijk)$], and stacking fault [$x=(111)$] and area factors $A_{(x)}/a_i^{02}$ for the surfaces and stacking fault. The lattice constant is a_i^0 .

	Structure	Z_d	$S_i^{(1),x}$	$S_i^{(2),x}$	$S_i^{(3),x}$	$A_{(x)}/a_i^{02}$
Perfect lattice	fcc	12	0	0	0	
	hcp	12	0	0	$\frac{1}{3}$	
	bcc	8	0	0	0	
	Diamond	4	0	0	$\frac{32}{9}$	
	Dimer	1	1	$\frac{2}{3}$	1	
Vacancy	fcc	11	1	$\frac{2}{3}$	1	
	bcc	7	1	$\frac{2}{3}$	1	
	Diamond	3	1	$\frac{2}{3}$	1	
(100) surface	fcc	8	8	$\frac{2}{3}$	5	$\frac{1}{2}$
	bcc	4	$\frac{16}{3}$	0	$\frac{112}{27}$	1
	Diamond	2	$\frac{4}{3}$	$\frac{8}{9}$	$\frac{52}{27}$	$\frac{1}{2}$
(111) surface	fcc	9	6	$\frac{3}{2}$	$\frac{15}{4}$	$\sqrt{3}/4$
	bcc	4	4	0	4	$\sqrt{3}$
		11	1	$\frac{2}{3}$	1	
		11	1	$\frac{2}{3}$	1	
(110) surface	Diamond	3	1	$\frac{2}{3}$	$\frac{25}{9}$	$\sqrt{3}/4$
	fcc	7	9	$\frac{2}{3}$	6	$\sqrt{2}/2$
	bcc	6	$\frac{8}{3}$	$\frac{8}{9}$	$\frac{56}{27}$	$\sqrt{2}/2$
(111) sf	Diamond	3	1	$\frac{2}{3}$	$\frac{25}{9}$	$\sqrt{2}/4$
	fcc	12	0	0	$\frac{1}{3}$	$\sqrt{3}/8$
	Diamond	4	0	0	$\frac{32}{9}$	$\sqrt{3}/8$

fect background densities $\bar{\rho}_i^x$ used in Eqs. (6) and (7) to calculate simple defect energies may be written in a simple form:

$$[\bar{\rho}_i^0(R)]^2 = \sum_{l=0}^3 t_i^{(l)} s_i^{(l),0} (\rho_i^{a(l)}(R))^2, \quad (10)$$

$$(\bar{\rho}_i^x)^2 = \sum_{l=0}^3 t_i^{(l)} s_i^{(l),x}. \quad (11)$$

The factors $s_i^{(l),0}$ and $s_i^{(l),x}$ depend only on geometry and are given in Table I and by $s_i^{(0),x} = Z_d^2$. Note that, for fcc and bcc, $\bar{\rho}_i^0 = Z_i \rho_i^{a(0)}(R)$, but for the diamond cubic and hcp (ideal c/a) lattices the $l=3$ component of the partial electron density enters into the reference lattice background electron density. For the perfect dimer and the vacancy in the three structures considered here, the $l=1-3$ contributions are identical. This same environment is also seen by the "second" atom at the low-density fcc and bcc surfaces. Only the $l=0$ and $l=3$ components contribute to the fcc stacking fault energy which has the same background electron density as the hcp perfect lattice with ideal c/a . The first-neighbor model does not distinguish the diamond cubic stacking fault, i.e., its energy is zero. Thus, the discrepancy in the original MEAM for silicon of a large stacking fault energy is not resolved here but is relegated to the consideration of longer-range interactions whose effect is determined by the details of the screening procedure and is not considered here. Note that the values for $s_i^{(l),x}$, $l=1,3$, are significantly larger for the free surface than the vacancy showing the importance of the correction terms in this case.

It is quite easy to obtain formulas for the energies of metastable structures. For any monatomic cubic structure with a center of symmetry, we obtain the following formula for the energy per atom:

$$E_i(R) = \frac{Z'}{Z_i} E_i^u(R) + \left[F_i(\rho_i^{a(0)}(R) Z' / Z_i) - \frac{Z'}{Z_i} F_i(\rho_i^{a(0)}(R)) \right], \quad (12)$$

where Z' is the number of nearest neighbors in the structure.

Calculation of shear elastic constants requires the second derivative of the total energy. For monatomic, centrosymmetric structures,

$$\frac{\partial^2 E_i}{\partial \epsilon^2} = \frac{1}{Z_i} \{ E_i^{u''} - F_i''(1) (\rho_i^{a(0)'})^2 \} \sum_{j(\neq i)} \left[\frac{\partial R_{ij}}{\partial \epsilon} \right]^2 + \frac{F_i'(1) t_i^{(2)}}{2Z_i^2} \frac{\partial^2 (\rho_i^{(2)})^2}{\partial \epsilon^2}, \quad (13a)$$

where ϵ is the shear mode (γ or γ') and the primes denote derivatives. For convenience, without loss of generality, we have taken the values of $t_i^{(0)}$ and of the atomic electron densities to be unity at equilibrium. The values for the R and ρ derivatives are given in Table II for the fcc and bcc structures. The expressions are considerably

TABLE II. Values of the derivatives of the atomic density $(\rho^{(2)})^{2''}$ and position $\sum(R')^2$ for the two shear modes. $\beta^{(2)}$ is the negative of the slope of $\rho_i^{a(2)}$ with respect to the scaled first-neighbor distance. [See Eq. (16) below.]

Shear mode	Structure	$(\rho^{(2)})^{2''}$	$\sum(R')^2$
γ	fcc	$4(\beta^{(2)}-2)^2$	1
	bcc	$\frac{256}{81}(\beta^{(2)}-1)^2$	$\frac{8}{9}$
γ'	fcc	$(\beta^{(2)}-6)^2$	$\frac{1}{2}$
	bcc	$\frac{256}{9}$	0

more complicated for the diamond cubic structure which also includes an internal relaxation. The shear elastic constants are easily obtained from Eq. (13a):

$$\gamma, \gamma' = \frac{\partial^2 E_i}{\partial \epsilon^2} / \Omega_i, \quad (13b)$$

where Ω_i is the atomic volume.

B. Determination of the parameters

We will now discuss the method for determining the parameters for specific elements. In this section we give detailed equations relating each parameter to a specific physical quantity. The casual reader is advised to skip this section and proceed to the applications in Sec. III. The reader who intends to develop his own MEAM functions will find this section invaluable. The formalism we use for the solid elements is also used for the gaseous elements. In the final subsection we describe how we obtain parameters for the gaseous elements. The resultant parameters are all given in Table III. Each subsection below includes an estimate of the reliability and uniqueness of the parameters.

It may seem as if there are an inordinate number of parameters for each element. In reality, for the pure solid elements there are 11 parameters, three of which we show below have little importance and are thus fixed at nominal values. Each of the eight remaining parameters is directly related to a physical quantity: the sublimation energy, the lattice constant, the bulk modulus, two shear constants, two structural energy differences, and the vacancy formation energy. These eight parameters are to be compared to the six or seven parameters used in the current formulations of the EAM (Refs. 27 and 28) or the seven used in the N -body formalism.¹⁶

1. Reference structure equation of state

The elements considered here have equilibrium solid phases at room temperature of the fcc ($Z_i=12$), bcc ($Z_i=8$), or diamond cubic ($Z_i=4$) crystal structure or are diatomic gases ($Z_i=1$). For the solid phases our method closely follows the procedure we have used previously.²⁷ The energy of an element in the reference structure is given by a universal energy function:³⁰

$$E_i^u(R) = -E_i^0(1+a^*)e^{-a^*}, \quad (14a)$$

$$a^* = \alpha_i (R_i / R_i^0 - 1), \quad (14b)$$

$$\alpha_i = \sqrt{9B_i \Omega_i / E_i^0}, \quad (14c)$$

or

$$\alpha_i = \sqrt{K_i / E_i^0 R_i^0}, \quad (14d)$$

where R_i^0 is the equilibrium nearest-neighbor distance, B_i is the bulk modulus, Ω_i is the atomic volume of the solid elements, and K_i is the diatomic force constant for the gaseous elements. Alternatively, we could use high-pressure experimental data or first-principles calculations to determine the reference structure equation of state.

In summary, we use the experimental values of the sublimation energy,³¹ nearest-neighbor distance,³² and bulk modulus,³³ or force constant³⁴ to determine the reference structure equation of state. The resultant parameters are very well determined, coming directly from clearcut experiments. Hence, the model gives excellent equilibrium properties. Away from equilibrium the model depends upon the universal equation of state which has been shown to be quite reasonable for $a^* > -1$.³⁰

2. Embedding function

The embedding function is chosen as a simple function of electron density:

$$F_i(\rho) = A_i E_i^0 \rho \ln \rho, \quad (15)$$

where A_i is a parameter to be determined. This logarithmic form has been shown previously²⁴ to give the correct coordination dependence between bond length and energy. We determine the value of A_i for the solid elements by using values of the fcc-bcc energy difference derived from phase diagrams³⁵ and Eq. (12). It should be noted that alternatively these energy differences could be obtained from *ab initio* local-density approximation (LDA) calculations. Currently the results of these two methods are somewhat in disagreement. The method of calculating the relaxed metastable energies is discussed in Sec. III below. We will see below that, when this structural energy difference is small, the values of A_i are expected to be close to unity for the bulk elements. Examination of Table III verifies our expectation. It turns out that, for the fcc elements, A_i is greater than unity and for the bcc elements A_i is less than or equal to unity. For carbon we also fit to the energy and lattice constants of graphite and this procedure results in a significantly higher value of A_i . We discuss below how we use experimental and theoretical trimer information³⁶⁻³⁹ to obtain A_i for the gaseous elements.

For the bulk elements the calculated structural energy difference is quite sensitive to the value of A_i , but unfor-

TABLE III. Parameters for the MEAM. Values listed are the sublimation energy E_i^0 (eV), the equilibrium nearest-neighbor distance R_i^0 (Å), the exponential decay factor for the universal energy function α_i , the scaling factor for the embedding energy A_i , the exponential decay factors for the atomic densities $\beta_i^{(l)}$, and the weighting factors for the atomic densities $t_i^{(l)}$.

	E_i^0	R_i^0	α_i	A_i	$\beta_i^{(0)}$	$\beta_i^{(1)}$	$\beta_i^{(2)}$	$\beta_i^{(3)}$	$t_i^{(0)}$	$t_i^{(1)}$	$t_i^{(2)}$	$t_i^{(3)}$
Cu	3.540	2.56	5.11	1.07	3.63	2.2	6.0	2.2	1	3.14	2.49	2.95
Ag	2.850	2.88	5.89	1.06	4.46	2.2	6.0	2.2	1	5.54	2.45	1.29
Au	3.930	2.88	6.34	1.04	5.45	2.2	6.0	2.2	1	1.59	1.51	2.61
Ni	4.450	2.49	4.99	1.10	2.45	2.2	6.0	2.2	1	3.57	1.60	3.70
Pd	3.910	2.75	6.43	1.01	4.98	2.2	6.0	2.2	1	2.34	1.38	4.48
Pt	5.770	2.77	6.44	1.04	4.67	2.2	6.0	2.2	1	2.73	-1.38	3.29
Al	3.580	2.86	4.61	1.07	2.21	2.2	6.0	2.2	1	-1.78	-2.21	8.01
Pb	2.040	3.50	6.06	1.01	5.31	2.2	6.0	2.2	1	2.74	3.06	1.20
Rh	5.750	2.69	6.00	1.05	1.13	1.0	2.0	1.0	1	2.99	4.61	4.80
Ir	6.930	2.72	6.52	1.05	1.13	1.0	2.0	1.0	1	1.50	8.10	4.80
Li	1.650	3.04	2.97	0.87	1.43	1.0	1.0	1.0	1	0.26	0.44	-0.20
Na	1.130	3.72	3.64	0.90	2.31	1.0	1.0	1.0	1	3.55	0.69	-0.20
K	0.941	4.63	3.90	0.92	2.69	1.0	1.0	1.0	1	5.10	0.69	-0.20
V	5.300	2.63	4.83	1.00	4.11	1.0	1.0	1.0	1	4.20	4.10	-1.00
Nb	7.470	2.86	4.79	1.00	4.37	1.0	1.0	1.0	1	3.76	3.83	-1.00
Ta	8.089	2.86	4.90	0.99	3.71	1.0	1.0	1.0	1	4.69	3.35	-1.50
Cr	4.100	2.50	5.12	0.94	3.22	1.0	1.0	1.0	1	-0.21	12.26	-1.90
Mo	6.810	2.73	5.85	0.99	4.48	1.0	1.0	1.0	1	3.48	9.49	-2.90
W	8.660	2.74	5.63	0.98	3.98	1.0	1.0	1.0	1	3.16	8.25	-2.70
Fe	4.290	2.48	5.07	0.89	2.94	1.0	1.0	1.0	1	3.94	4.12	-1.50
C	7.370	1.54	4.31	1.80	5.50	4.3	3.1	6.0	1	5.57	1.94	-0.77
Si	4.630	2.35	4.87	1.00	4.40	5.5	5.5	5.5	1	3.13	4.47	-1.80
Ge	3.850	2.45	4.98	1.00	4.55	5.5	5.5	5.5	1	4.02	5.23	-1.60
H	2.225	0.74	2.96	2.50	2.96	3.0	3.0		1	0.20	-0.10	0.00
N	4.880	1.10	5.96	1.50	4.00	4.0			1	0.05	0.00	0.00
O	2.558	1.21	6.49	1.50	6.49	6.5	6.5		1	0.09	0.10	0.00

tunately there is considerable uncertainty about the correct structural energy. For the gaseous elements the amount of data fit is small and the value of A_i is not well determined.

3. Atomic electron densities

The equations for the atomic electron densities are assumed to be given by a simple exponential form:

$$\rho_i^{a(l)}(R) = e^{-b^*}, \quad (16a)$$

$$b^* = \beta_i^{(l)}(R/R_i^0 - 1), \quad (16b)$$

where $\beta_i^{(l)}$, $l=0-3$ are parameters to be determined. Note that, without loss of generality, we have chosen the form so that at equilibrium each atomic electron density is equal to unity. Banerjee and Smith⁴⁰ have shown that a simple exponential represents the electron density quite well for the bulk, near vacancies and free surfaces, and for diatomics.

To determine the values of $\beta_i^{(l)}$, $l=0-3$, we first use the experimental shear elastic constants.³³ From Eq. (13) we see that the shear elastic constants for the fcc and bcc structures depend upon only the $l=0$ and $l=2$ atomic electron densities. It was found that the specific values of the exponential decay constant $\beta_i^{(2)}$ do not severely affect most calculated properties, so for simplicity $\beta_i^{(2)}$ was chosen to eliminate the $l=2$ contribution to one of the shear elastic constants (see Table II). That is, for fcc materials, $\beta_i^{(2)}$ was chosen equal to either 2 or 6 (depending upon the experimental shear elastic constants) and for bcc materials $\beta_i^{(2)}$ was chosen equal to 1. Then for fcc and bcc materials using Eq. (13) and Table II, $\beta_i^{(0)}$ is uniquely determined by the shear elastic constants:

$$\beta_i^{(0)} = \left[\frac{\alpha_i^2 - 2Z_i\gamma'\Omega_i/E_i^0}{A_i} \right]^{1/2} \quad \text{for } \beta_i^{(2)} = 6, \quad (17a)$$

$$\beta_i^{(0)} = \left[\frac{\alpha_i^2 - Z_i\gamma\Omega_i/E_i^0}{A_i} \right]^{1/2} \quad \text{for } \beta_i^{(2)} = 2, \quad (17b)$$

$$\beta_i^{(0)} = \left[\frac{\alpha_i^2 - 9Z_i\gamma\Omega_i/8E_i^0}{A_i} \right]^{1/2} \quad \text{for } \beta_i^{(2)} = 1. \quad (17c)$$

[Because of the lack of data for the diamond cubic and dimer structures, we take $\beta_i^{(1)} = \beta_i^{(2)} = \beta_i^{(3)}$ except for carbon where graphite stability and geometry are used. In the case of the diamond cubic elements, we use a numerical procedure²⁴ to calculate the shear elastic constants and vary $\beta_i^{(0)}$ and $\beta_i^{(1)}$ until we get agreement with experiment. It is found that, for the values of β in Table III for silicon, the first-neighbor relaxation to a vacancy is outward (0.05 Å) in agreement with initial first-principles calculations⁴¹ but not more recent calculations²⁵ and the relaxation at unreconstructed low index free surfaces is slightly outward (0.05–0.1 Å) in disagreement with first-principles calculations⁴² which show a small inward relaxation. These relaxations do depend, although insensitively, upon the values of β used. It is likely that variation of $\beta_i^{(1)}$, $\beta_i^{(2)}$, and $\beta_i^{(3)}$ could improve agreement with the first-principles calculations. The calculated relaxations at the silicon surfaces are significantly smaller than

those previously reported²⁴ using the MEAM. We discuss below how we use experimental and theoretical trimer information^{36–39} to obtain $\beta_i^{(l)}$ for the gaseous elements.

For the fcc and bcc elements we find that the relaxation near a vacancy and free surface depend upon the values of $\beta_i^{(l)}$, $l=1$ and 3. This effect is expected due to the loss of mirror-plane symmetry. We choose a value of $\beta_i^{(1)} = \beta_i^{(3)}$ to insure that these relaxations are small ($\sim < 0.1$ Å) and into the vacancy and away from the free surface. For these calculations we use the screening procedure described in the Appendix.

In general, the values of the $\beta_i^{(l)}$ are not well determined because they are highly correlated and we have chosen some of them somewhat arbitrarily. However, the experimental elastic constants restrict their values to a limited range. On the other hand, small variations in the chosen values do not seem to be particularly important in the calculations that we present below. We have no reason to expect that this insensitivity is a general result. Choosing $\beta_i^{(l)}$ to agree with the slope of the actual atomic densities, as we have done previously,⁵ was not tried here. Johnson¹⁸ in his analytic first-neighbor EAM for Cu found that an electron density decay constant of 6.0 yielded reasonable functions but could not fit both shear elastic constants. This value should be compared with the calculated angular momentum averaged atomic values for the $3d^{10}4s^1$ state of 6.0 and $3d^94s^2$ of 6.6. Our values for Cu (see Table III) are 3.63, 2.2, 6.0, and 2.2 for $l=0-3$ (*spdf*).

It is in the selection of the β 's that the functions presented here are not optimized. Before significant use is made of these functions, it is recommended that a more definitive evaluation of the β 's be made using either first-principles calculations of the volume dependence of the shear elastic constants, experimental vacancy, or surface relaxation data, experimental higher-order elastic constant data, or phonon dispersion data.

4. Partial electron density weights

The final parameters are the weighting functions $t_i^{(l)}$ for the partial electron density used in Eq. (9). As discussed above, $t_i^{(0)} = 1$. The values of $t_i^{(2)}$ for the fcc and bcc elements are determined from the elastic shear constants³³ using Eq. (13) and Table II:

$$t_i^{(2)} = \frac{(\gamma - 2\gamma')Z_i^2\Omega_i}{2A_iE_i^0(\beta_i^{(2)} - 2)^2} \quad \text{for } \beta_i^{(2)} = 6, \quad (18a)$$

$$t_i^{(2)} = \frac{(2\gamma' - \gamma)Z_i^2\Omega_i}{A_iE_i^0(\beta_i^{(2)} - 6)^2} \quad \text{for } \beta_i^{(2)} = 2, \quad (18b)$$

$$t_i^{(2)} = \frac{9\gamma'Z_i^2\Omega_i}{256A_iE_i^0} \quad \text{for bcc.} \quad (18c)$$

For the diamond cubic elements, $t_i^{(2)}$ is determined by the numerical procedure discussed above. The values of $t_i^{(2)}$ are all positive except for Pt and Al and range from ≈ 0.5 for Li, Na, and K to ≈ 10 for Cr, Mo, and W. There seems to be a regular parabolic behavior in $t_i^{(2)}$ based on

the number of d electrons (see Fig. 1) as is seen in many d -band properties.¹ For the bulk elements, $t_i^{(3)}$ is determined uniquely from Eq. (7) by the experimental stacking fault energy⁴³ or structural energy difference between the fcc and hcp phases.³⁵ For the fcc elements $t_i^{(3)}$ must be greater than zero while for the bcc and diamond cubic elements $t_i^{(3)}$ is less than zero. Once the $t_i^{(l)}$, $l=0,2,3$, are determined, $t_i^{(1)}$ is uniquely determined from Eq. (6) and the experimental⁴⁴⁻⁴⁸ or calculated⁴⁹ vacancy formation energy. The values of $t_i^{(1)}$ are all positive except for Al and Cr. It has been assumed in these calculations that the relaxation energy is negligible. It would be a simpler matter to include relaxation iteratively. The correction of the $l=1-3$ partial densities to the dominant EAM density scales as $t_i^{(1)}/Z_i^2$. Since the $t_i^{(l)}$ are usually all of order unity, the correction scales inversely with coordination of the reference lattice squared and is small for the fcc elements, significant for the bcc's and crucial for the diamond cubics and dimers. This behavior correlates well with our success in using the EAM for fcc's, our limited success with bcc's, and the necessity to use the MEAM for diamond cubics.

The determination of $t_i^{(l)}$ is definitive for the cases that depend on the elastic constants or stacking fault energies. In the case of $t_i^{(1)}$, which depends on the vacancy formation energy, the value is only as good as the experimental data which is sometimes not well determined. Similarly, the structural energy differences between the fcc and hcp phases is questionable.

5. Parameters for the gaseous elements

The determination of the parameters for the diatomic molecules is less definitive than that for the solid elements due to the minimal amount of experimental and theoretical information that has been used. In principle, high-quality quantum chemistry calculations could be performed to definitively establish the MEAM parameters. We have used experimental data³⁶ and calculations³⁷⁻³⁹

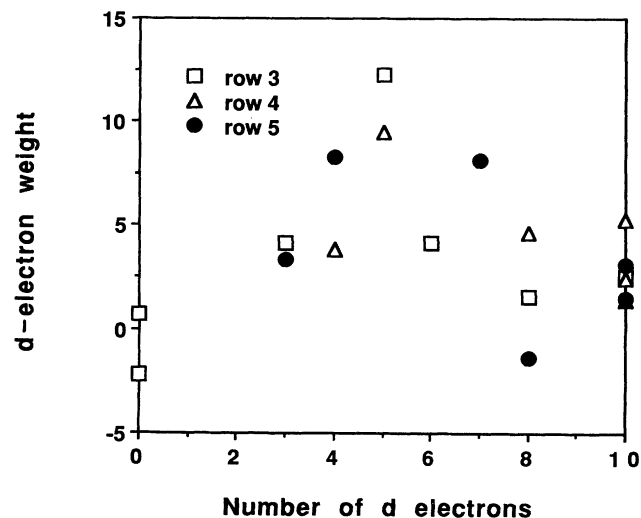


FIG. 1. Weighting parameter for $l=2$ (d electrons) $t_i^{(2)}$ vs number of d electrons. The specific row in the Periodic Table for each element is indicated.

for trimers of various geometry to determine our parameters. In Fig. 2 we present the results of fitting to the trimer information. In general, we considered three trimer geometries, the equilateral triangle, where there is no screening, and the linear and $\approx 120^\circ$ trimers, where the two outside atoms are completely screened (see the Appendix for a discussion of screening).

For hydrogen, the first-principles calculations of Siegbahn and Liu³⁷ were used. These calculations predict the linear trimer to be the lowest metastable equilibrium with an atomic separation of 0.93 Å and an energy 0.42 eV above that of an isolated hydrogen atom and dimer. The 120° trimer and equilateral triangle are predicted to have an equilibrium atom separations of 0.95 and 1.06 Å, respectively, and energies 0.29 and 2.3 eV above the linear geometry minimum configuration. Note that the MEAM calculations for the equilateral triangle yield an atomic separation somewhat greater than the first-principles calculations.

For nitrogen, the equilibrium trimer was fit to the linear experimental geometry with a relative separation R_{ij}/R_i^0 of 1.075 and an energy between -9.8 and -14.3 eV.³⁶ Since so little data have been used, the density weighting parameters for $l=2,3$ were set equal to zero for simplicity. It is necessary to have $t_i^{(1)} > 0$ to have the linear trimer more stable than the 120° bent trimer.

For oxygen the equilibrium geometry is a 116.8° trimer with atom separation of 1.28 Å and an energy 1.04 eV below that of an isolated oxygen atom and dimer.³⁶ The equilateral triangle configuration has an atomic spacing of 1.45 Å and an energy 1.22 eV above the 116.8° trimer.³⁸ The minimum at the bent geometry is attained not through repulsion of the outside atoms, which are completely screened, but through a tradeoff between the $l=1$ and $l=2$ partial electron density contributions.

We conclude this section by presenting in Table IV the calculated shear elastic constants, unrelaxed vacancy formation energies, and stacking fault energies that result from the MEAM using the parameters in Table III. For all of the elements, the calculated values are almost exactly equal to the experimental or theoretical input except for the diamond cubic structure where the elastic constants are within a few percent of the experimental input. For the latter elements the predicted internal relaxation parameter is also given. For both Si and Ge we obtain a value of 0.75 which is in excellent agreement with experiment of 0.74 for Si (Ref. 50) and 0.71 for Ge.⁵¹ For carbon a much larger value of the internal relaxation parameter is obtained; unfortunately, there is no experimental data available for comparison. As discussed above, the stacking fault energy for the diamond cubic materials is zero for the first-neighbor model.

III. APPLICATION TO SURFACES AND METASTABLE STRUCTURES

The surface energy is an important physical quantity that may be readily compared with experiment. However, it should be noted that this comparison is somewhat complicated. Experimental surface energies depend strongly upon impurities and must be extrapolated to 0 K

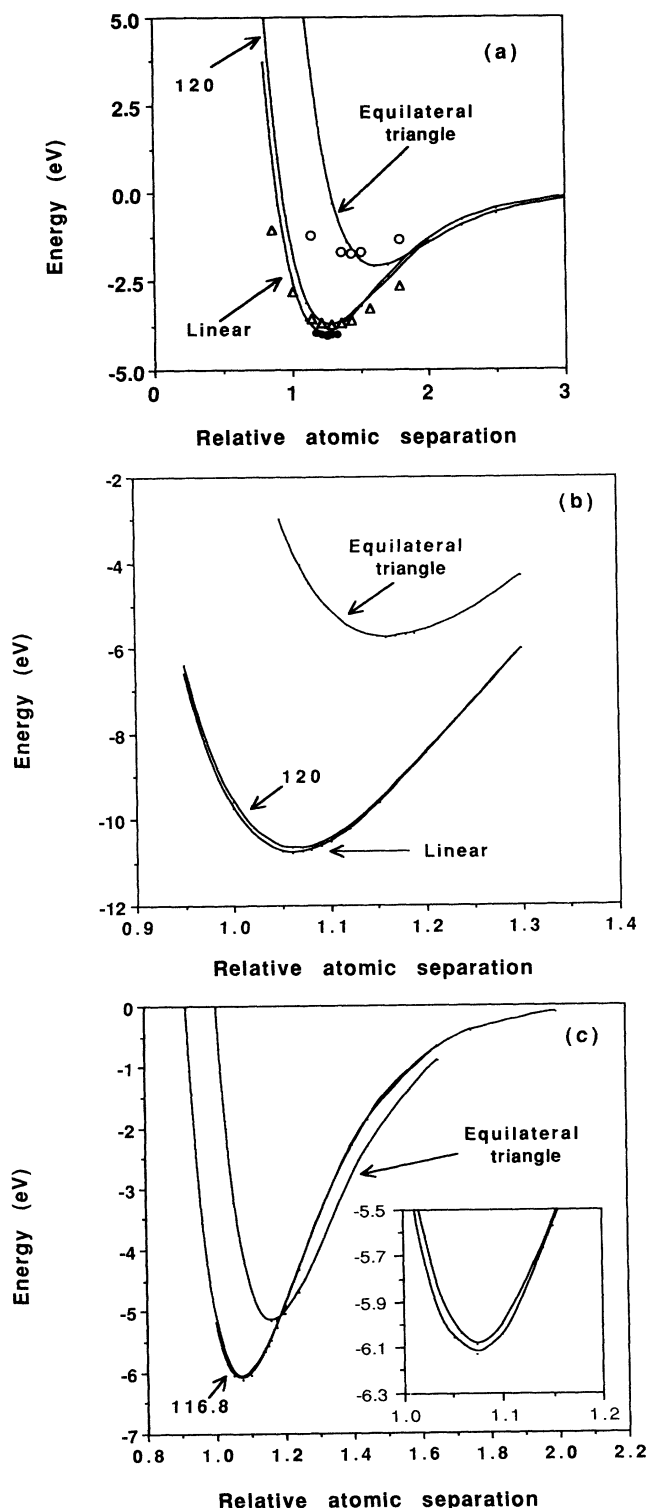


FIG. 2. (a) Trimer energy (eV) for hydrogen vs relative atomic separation R_{ij}/R_i^0 . Symbols represent calculations of Hay and Dunning (Ref. 37). The curve labeled "120" is for a bent trimer with a 120° angle between the three atoms. (b) Trimer energy (eV) for nitrogen vs relative atomic separation R_{ij}/R_i^0 . The curve labeled "120" is for a bent trimer with a 120° angle between the three atoms. (c) Trimer energy (eV) for oxygen vs relative atom separation R_{ij}/R_i^0 . The linear configuration lies just above the bent 116.8° metastable trimer as shown in the inset.

to be compared to calculations. In addition, it has been pointed out⁵² that perhaps surface stress rather than energy should be compared to experiment. Using Eq. (7) we calculate the surface energy which depends strongly upon the surface background electron density $\bar{\rho}_i^{(x)}$. In Fig. 3, we present results for the relative surface electron density and in Table V we present the results for the surface energy. The ratio $\bar{\rho}_i^{(x)}/Z_i$ gives an indication of the amount of "missing" electron density at the surface. We see that, on the close-packed surfaces for both fcc and bcc, the surface electron density is predicted to be the highest. The densities for Cr, Li, and Au appear lower than the corresponding elements in the same column of the Periodic Table. We see from the predicted energies in Table V that the agreement, in most cases, with polycrystalline experimental data^{53,54} is quite good. The lowest-energy single-crystal surface is expected to be reasonably close to the polycrystalline data. The worst agreement occurs for Cr and Au for which we noted above have anomalously low surface electron densities. For the fcc metals, the high atomic density (111) surface is predicted to have the lowest energy with the (100) and (110) energies slightly higher. In a few cases the low-density (110) surface energy is higher than the (100) surface energy. This effect has also been calculated by Smith and Banerjee.¹⁹ For the bcc metals, the high-density (110) surface is predicted to have the lowest energy except in the case of Mo. Surprisingly, the (111) surface is predicted to have a lower energy than the closer-packed (100) surface. Both Si and Ge yield calculated surface energies greater than experiment. In all cases the surface energy depends strongly upon the experimental vacancy formation energy used. In many cases this energy is not known well. Fu *et al.*⁵⁵ have used density-functional theory to calculate the (100) surface energy in W and V. Their calculated value for W of 5100 erg/cm² is considerably higher than the value calculated here, but their value for V of 3400 erg/cm² is much closer to the value calculated here.

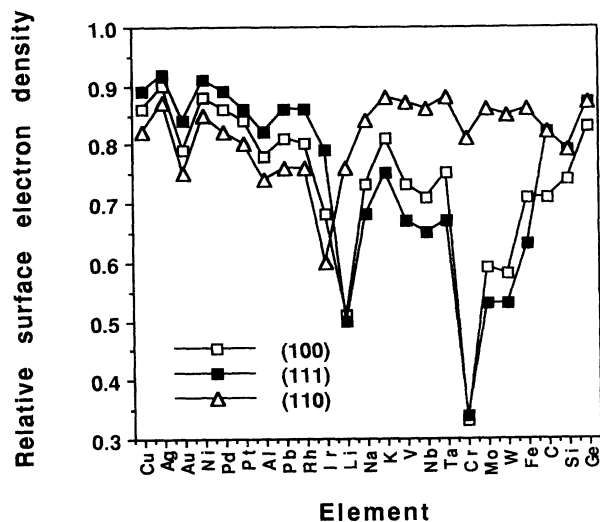


FIG. 3. Relative surface electron density $\bar{\rho}_i^{(x)}/Z_i$ for three low index surfaces.

It should be noted that, in their paper, they quote experimental values for W of 1800–5000 ergs/cm², so that the correct surface energy is far from established. Previous EAM calculations²⁷ for the fcc elements yielded single-crystal surface energies as much as 50% below the polycrystalline experimental values. It appears that the MEAM yields surface energies that are closer in line with what is expected for single-crystal energies.

We derived in Eq. (12) above the general expression for the energy of an atom in a monatomic centrosymmetric lattice with Z' nearest neighbors. For the specific equation of state [Eq. (14)] and embedding function [Eq. (15)] chosen above we obtain

$$E_i(R') = \frac{Z'E_i^0}{Z_i} \{ -(1+a^*)e^{-a^*} + A_i\rho^{\alpha(0)} \ln(Z'/Z_i) \}, \quad (19)$$

where a^* and $\rho^{\alpha(0)}$ are functions of the nearest-neighbor distance R' . By taking the derivative of Eq. (19) with respect to nearest-neighbor distance, we obtain an iterative equation for the relaxed nearest-neighbor distance R' of the metastable structure with Z' nearest neighbors:

$$\Delta r = \frac{\beta_i^{(0)} A_i \ln(Z'/Z_i) e^{-(\beta_i^{(0)} - \alpha_i)\Delta r}}{\alpha_i^2}, \quad (20)$$

TABLE IV. Calculated values of the shear elastic constants γ and γ' (eV/Å³), the unrelaxed vacancy formation energy E_v^f (eV), and the unrelaxed stacking fault energy E_{sf}^f (ergs/cm²). The parameters of the MEAM were determined from these experimental quantities, when known, and agree to better than a few percent. The values of the internal relaxation parameter ξ are given in parentheses for the diamond cubic materials.

	γ	γ'	E_v^f	E_{sf}^f
Cu	0.47	0.15	1.14	73
Ag	0.29	0.10	1.02	20
Au	0.26	0.091	0.90	55
Ni	0.78	0.31	1.46	125
Pd	0.45	0.18	1.40	100
Pt	0.48	0.30	1.30	110
Al	0.17	0.14	0.67	160
Pb	0.093	0.023	0.58	9
Rh	1.21	0.72	2.70	172
Ir	1.68	1.07	3.50	203
Li	0.060	0.007	0.34	
Na	0.027	0.004	0.42	
K	0.012	0.002	0.42	
V	0.32	0.34	2.30	
Nb	0.25	0.35	2.95	
Ta	0.52	0.33	3.30	
Cr	0.63	0.88	1.95	
Mo	0.69	0.91	3.40	
W	0.98	0.98	3.87	
Fe	0.73	0.30	1.95	
C	2.33(5.4)	1.40	7.00	0
Si	0.48(0.75)	0.31	4.00	0
Ge	0.43(0.75)	0.25	4.00	0

where $\Delta r = R'/R_i^0 - 1$. We may obtain an estimate of the energy of structures near the reference structure by considering the case of structures where $Z' \approx Z$. Then, using Eqs. (19) and (20),

$$E_i(R') = E_i^0 \{ -1 + (A_i - 1)\Delta + \frac{1}{2} A_i [1 - A_i (\beta_i^{(0)} / \alpha_i)^2] \Delta^2 + o(\Delta^3) \}, \quad (21)$$

where $\Delta = Z'/Z - 1$. If the reference structure ($\Delta = 0$) is to have the minimum energy, then we expect that $A_i = 1$ and $\beta_i^{(0)} < \alpha_i / \sqrt{A_i}$. In reality, Z' takes on discrete values so that it is only necessary that $A_i \approx 1$ to assure that the reference structure has the minimum energy.

Using the above equations, we have calculated the energy and relative change in equilibrium nearest-neighbor distance for all of the elements considered above. The results are presented in Table VI. The hcp phase was calculated assuming an ideal c/a ratio. Note that the MEAM is able to represent the experimental structural energies quite well. We note a potential problem with the predicted stability of some of the bcc elements in the simple-cubic and diamond cubic structures. Even though the bcc structure is predicted to be the equilibrium phase, the energies of these metastable phases are only a few hundredths of an eV higher. Recent density-functional calculations⁵⁶ predict that the energy of the simple-cubic and diamond cubic structures of 3d metals are on the or-

TABLE V. Calculated values of the surface energy for low index crystal faces compared to the experimental polycrystalline average values (ergs/cm²). The experimental values (Refs. 53 and 54) are accurate at least to about 10% and in a number of cases, indicated by an asterisk, have been crudely extrapolated from the melt temperature to 0 K.

	(110)	(111)	(110)	expt
Cu	1651	1409	1642	1770
Ag	1271	1087	1222	1320
Au	1084	886	1115	1540
Ni	2435	2036	2384	2240
Pd	1659	1381	1670	2000*
Pt	2167	1656	2131	2500*
Al	897	618	969	1000 ⁵⁴
Pb	424	366	431	600*
Rh	2902	2598	2921	2600*
Ir	2907	2835	3058	3000*
Li	431	279	202	520*
Na	288	202	169	260*
K	182	125	110	145*
V	2490	1805	1705	2600*
Nb	2788	2018	1868	2300*
Ta	3292	2305	2173	2780*
Cr	1230	1247	1032	2200*
Mo	2122	1861	1930	2900*
W	2646	2247	2232	2990
Fe	2289	1720	1566	2360
C	6195	5082	6224	
Si	1878	1253	1535	1135*
Ge	1658	1154	1414	900*

der of eV's above the bcc structure. It should be noted that Paxton, Methfessel, and Polatoglou⁵⁶ significantly overestimate the fcc-bcc energy difference of the 3d metals compared to the presumably more accurate phase diagram³⁵ results. Volume changes, however, seem to be in agreement with these calculations. For V, both Paxton, Methfessel, and Polatoglou⁵⁶ and the present calculations give the ratio of the diamond cubic to bcc atomic volumes as 1.4.

For hydrogen the value of $\Delta r = 10$ means that no metastable solid structure with the indicated symmetry was found at zero pressure. Stable structures for nitrogen and oxygen were found to lie within a few eV's of the dimer energy. Molecular solids were not considered. We see that, as expected, in all cases the equilibrium nearest-neighbor distance decreases as we go from the close-packed structure to a lower coordination.

As mentioned above for carbon, the graphitic structure was also fit. The resultant calculated (experimental) equilibrium structure has an energy 5 (10) meV below that of diamond, an in-plane nearest-neighbor distance of 0.92 (0.92) of that of diamond, and interplanar spacing of 3.3 (4.4) diamond nearest-neighbor distances. The potential-energy surface normal to the graphite planes is quite flat

and very small parameter changes can affect the equilibrium geometry and energy significantly.

IV. APPLICATION TO BINARY SYSTEMS

In our previous work we applied the EAM to impurity^{4,5} and alloy systems.²⁷ In that work we used the experimental values of the dilute heats of solution to scale the electron density and determined the unlike-atom pair potential by assuming a geometric mean between the like-atom potentials. In this work a different tack more in the direction of that used by Voter and Chen,²⁸ and parallel to the method used above to obtain the monatomic pair potential, is used. Instead of considering a dilute alloy system, consider an equiatomic binary intermetallic alloy system (ij) where each i atom has only j neighbors and vice versa. Simple examples of these systems are the $B1$ (NaCl type-6 neighbors) or $B2$ (CsCl type-8 neighbors) crystal structures. For such a reference lattice which is cubic and has a center of symmetry, the total energy per atom ($\frac{1}{2}$ i atom + $\frac{1}{2}$ j atom) $E_{ij}^H(R)$ is given by

$$E_{ij}^H(R) = \frac{1}{2} [F_i(Z_{ij}\rho_j^a(0)(R)/Z_i) + F_j(Z_{ij}\rho_i^a(0)(R)/Z_j) + Z_{ij}\phi_{ij}(R)], \quad (22)$$

TABLE VI. Calculated structural energy differences (eV) and relative changes in nearest-neighbor distances. The energies are relative to the equilibrium phase except for hcp, where the energy is relative to the fcc structure. When two energies are listed, the first is the MEAM calculation and the second is the energy derived from the experimental stacking fault (Ref. 43) or phase diagram information (Ref. 35). The parameter A_i has been varied to yield agreement with this latter energy.

	fcc		hcp		bcc		sc		Diamond			
	ΔE	Δr										
Cu			0.013	0.006	0.04	0.04	-0.06	0.20	-0.09	0.75	-0.13	
Ag			0.005	0.003	0.03	0.03	-0.05	0.15	-0.08	0.46	-0.12	
Au			0.012	0.005	0.02	0.04	-0.05	0.12	-0.09	0.59	-0.14	
Ni			0.021	0.015	0.09	0.07	-0.04	0.38	-0.06	1.13	-0.09	
Pd			0.020	0.020	0.10	0.10	-0.05	0.28	-0.08	0.95	-0.11	
Pt			0.023	0.020	0.12	0.15	-0.04	0.40	-0.07	1.27	-0.11	
Al			0.036	0.050	0.11	0.10	-0.04	0.36	-0.07	1.22	-0.10	
Pb			0.003	0.003	0.03	0.02	-0.06	0.09	-0.09	0.27	-0.14	
Rh			0.034	0.030	0.27	0.19	-0.01	0.76	-0.02	1.70	-0.03	
Ir			0.040	0.040	0.33	0.32	-0.01	0.92	-0.02	2.05	-0.03	
Li	0.01	0.00	0.06	-0.001	-0.001			0.09	-0.04	0.29	-0.09	
Na	0.01	0.00	0.07	-0.000	-0.001			0.05	-0.04	0.16	-0.10	
K	0.01	0.00	0.07	-0.000	-0.000			0.04	-0.04	0.12	-0.10	
V	0.13	0.15	0.08	-0.012	-0.060			0.06	-0.05	0.12	-0.11	
Nb	0.11	0.22	0.08	-0.017	-0.050			0.05	-0.05	0.01	-0.13	
Ta	0.28	0.26	0.07	-0.027	-0.060			0.15	-0.04	0.03	-0.09	
Cr	0.12	0.09	0.05	-0.017	-0.020			0.15	-0.03	0.36	-0.07	
Mo	0.23	0.28	0.06	-0.045	-0.050			0.12	-0.04	0.02	-0.08	
W	0.32	0.33	0.05	-0.053	-0.060			0.20	-0.03	0.28	-0.08	
Fe	0.03	-0.02	0.05	-0.013	-0.030			0.21	-0.03	0.48	-0.06	
C	1.11	1.20	0.37	0.000	-0.030	1.37	1.14	0.27	1.33	0.18		
Si	0.53	0.51	0.23	-0.007	-0.010	0.48	0.47	0.14	0.58	0.08		
Ge	0.38	0.36	0.22	-0.006	-0.030	0.36	0.34	0.13	0.44	0.08		
H	2.24		10			2.24		10	2.24	10		
N	3.62		0.63	0.000		3.29		0.52	3.01	0.45	2.54	0.34
O	2.04		0.57	0.000		1.86		0.48	1.71	0.41	1.43	0.32

where Z_{ij} is the number of nearest neighbors to an i or j atom. As above, we solve for the pair potential assuming that the equation of state is known. Then

$$\phi_{ij}(R) = \frac{1}{Z_{ij}} [2E_{ij}^u(R) - F_i(Z_{ij}\rho_i^{a(0)}(R)/Z_i) - F_j(Z_{ij}\rho_j^{a(0)}(R)/Z_j)] . \quad (23)$$

As in Eq. (14), we use the universal form³⁰ for the intermetallic energy with parameters $E_{ij}^0 = (E_i^0 + E_j^0)/2 - \Delta_{ij}$, $\alpha_{ij} = (\alpha_i + \alpha_j)/2$, and R_{ij}^0 calculated from the assumed equilibrium intermetallic atomic volume $\Omega_{ij} = (\Omega_i + \Omega_j)/2$. For the binaries of a solid with a gaseous impurity, the reference state is taken as the solid element with interstitial impurities (no relaxation). These obvious simplifications are not necessary but allow a simple qualitative test to the model. Alternatively we could use experimental or calculated values for the intermetallic energy if they are known. We obtain approximate calculated values of the enthalpy of mixing Δ_{ij} from de Boer *et al.*⁵⁷ for the solid elements and experimental values from handbooks^{33,58} for the impurities and list these values in Tables VII-IX. In de Boer *et al.*⁵⁷ these calculated values are found to agree quite well with experiment when available. Negative entries indicate an exothermic heat of mixing. It turns out that some of the dilute heats of solution for hydrogen are readily available.⁵⁹ Thus, in

these cases, we back calculate Δ_{ij} from the unrelaxed dilute heat of solution using the approximations discussed below. These values are underlined in Tables VII-IX. We choose to use a reference lattice of B2 type ($Z_{ij} = 8$) for the solid-solid alloys although this choice is found to be unimportant. We do not consider the case of mixed gaseous elements although a similar formalism to that used above based on a mixed dimer reference state could be used.

As a first approximation we assume that the partial electron density *weights* depend only on the embedded atom type and not on the type of the atom contributing the density. In addition, to facilitate calculations without any additional parameters, we do not scale the electron densities as we have done previously.²⁷ The reader should be cautioned that these assumptions are extreme and that much better potentials could be obtained by scaling the electron density. If detailed calculations are to be performed it is recommended that experimental heats of solution be used to scale the densities. In addition, the assumption made above about the partial electron density weights needs to be fully investigated.

We present in Table X the results of calculations of the dilute heats of solution for the elements for which alloy data is available in the fcc elements. In these calculations relaxation of only the first shell of neighbors to the fcc or bcc substitutional impurity atom has been performed.

TABLE VII. Literature values of calculated or experimental heats of formation (eV/atom) Δ_{ij} for equiatomic compounds of fcc elements with other elements. No entry indicates that data were not available. Underlined values are derived from the dilute heats of solution.

	Cu	Ag	Au	Ni	Pd	Pt	Al	Pb	Rh	Ir
Cu				0.05	-0.20	-0.18			-0.04	0.00
Ag				0.23	-0.11	-0.01			0.14	0.22
Au				0.11	0.00	0.07			0.11	0.17
Ni	0.05	0.23	0.11		0.00	-0.07	-0.48	0.02	-0.01	-0.02
Pd	-0.20	-0.11	0.00	0.00		0.03	-0.84	-0.46	0.03	0.09
Pt	-0.18	-0.01	0.07	-0.07	0.03		-0.82	-0.27	-0.02	0.01
Al				-0.48	-0.84	-0.82			-0.64	-0.60
Pb				0.02	-0.46	-0.27			-0.10	0.05
Rh	-0.04	0.14	0.11	-0.01	0.03	-0.02	-0.64	-0.10		0.01
Ir	0.00	0.22	0.17	-0.02	0.09	0.01	-0.60	0.05	0.01	
Li				0.01	-0.58	-0.47			-0.20	-0.13
Na				0.46	-0.21	-0.01			0.28	0.41
K				0.59	-0.12	0.12			0.42	0.58
V	0.07	0.25	-0.29	-0.27	-0.53	-0.68	-0.40	0.04	-0.44	-0.51
Nb	0.04	0.25	-0.48	-0.45	-0.79	-1.00	-0.44	0.05	-0.68	-0.80
Ta	0.03	0.21	-0.45	-0.44	-0.78	-0.98	-0.46	0.02	-0.67	-0.78
Cr	0.19	0.40	0.00	-0.10	-0.22	-0.36	-0.30	0.23	-0.20	-0.27
Mo	0.27	0.52	0.05	-0.11	-0.22	-0.42	-0.24	0.42	-0.23	-0.32
W	0.33	0.60	0.16	-0.05	-0.10	-0.30	-0.30	0.53	-0.14	-0.23
Fe	0.19	0.42	0.12	-0.02	-0.06	-0.19	-0.32	0.25	-0.08	-0.13
C				0.21	0.32	0.34	-0.32		0.27	0.32
Si				-0.45	-0.57	-0.56			-0.44	-0.40
Ge				-0.20	-0.51	-0.43			-0.31	-0.23
H	<u>0.28</u>	<u>0.29</u>	<u>0.14</u>	<u>0.09</u>	<u>-0.05</u>				<u>0.14</u>	<u>0.38</u>
N	0.25			0.36	0.48	0.62	-1.60		0.46	0.59
O	-0.78	-0.12		-1.20	-0.56		-3.50	-1.10	-0.79	-0.90

For the case of the gaseous impurities, an interstitial geometry is used and no relaxation is allowed. Screening is accomplished using the procedure defined in the Appendix except for the case of the interstitial where, because of its small electron density, screening due to the interstitial has been ignored. The direct comparison to experiment when available is shown in Fig. 4. Even though the trend is correct, the agreement between experiment and calculation is only fair. Note that almost all of the calculated heats are more negative than experiment. This disagreement occurs because the electron densities are not scaled; that is, every type of atom has the same electron density at its equilibrium separation. By varying this ratio we make the local environment of a host atom less hostlike and thus raise the heat of solution. Therefore, we could obtain better agreement with experiment by scaling the electron densities. For example, consider the five cases of Ni, Pd, and Pt in Cu, and Cu in Ni and Pd where experimental dilute heats of solution are available. By simply reducing the electron density of Cu (relative to Ni, Pd, and Pt) by a factor of 2 and using the relaxation energies obtained above, the heats of solution (eV) are calculated to be 0.09(0.03), $-0.28(-0.44)$, $-0.63(-0.53)$, 0.15(0.11), and $-0.50(-0.39)$ where the experimental values are given in parentheses. This agreement is excellent. In the cases where the relaxation is large we have chosen not to report the dilute heats of

solution as the relaxation procedure used here was deemed insufficient to yield a close approximation to the fully relaxed value. In the remaining substitutional cases the relaxation is accurate to better than ≈ 0.1 eV. It is easily shown that, for the simplifying assumptions above, to a good approximation the dilute heat of solution for the interstitials is given by $2\Delta_{ij}$. The value calculated for substitutional carbon in solution appear quite large certainly to some extent because relaxation has not been included and more importantly because the interstitial geometry is the equilibrium state. Similarly, the solution energies for silicon and germanium in nickel are large.

From elasticity theory, the relaxation energy is expected to depend upon the relative difference in volume of the host and impurity. In Fig. 5 we show this dependence. Here we have plotted the relaxation energy, normalized by the host bulk modulus times atomic volume, versus the relative volume difference squared. Elasticity theory predicts that, if the volume contribution to the relaxation energy were dominant, the points would lie on a straight line. Even though some linear dependence may be seen for specific hosts, clearly there are important chemical effects in addition to the volume effect.

V. SUMMARY

The following outline summarizes the main contributions of this manuscript.

TABLE VIII. Literature values of calculated or experimental heats of formation (eV/atom) Δ_{ij} for equiatomic compounds of bcc elements with other elements. No energy indicates that data were not available. Underlined values are derived from the dilute heats of solution.

	Li	Na	K	V	Nb	Ta	Cr	Mo	W	Fe
Cu				0.07	0.04	0.03	0.19	0.27	0.33	0.19
Ag				0.25	0.25	0.21	0.40	0.52	0.60	0.42
Au				-0.29	-0.48	-0.45	0.00	0.05	0.16	0.12
Ni	0.01	0.46	0.59	-0.27	-0.45	-0.44	-0.10	-0.11	-0.05	-0.02
Pd	-0.58	-0.21	-0.12	-0.53	-0.79	-0.78	-0.22	-0.22	-0.10	-0.06
Pt	-0.47	-0.01	0.12	-0.68	-1.00	-0.98	-0.36	-0.42	-0.30	-0.19
Al				-0.40	-0.44	-0.46	-0.30	-0.24	-0.20	-0.32
Pb				0.04	0.05	0.02	0.23	0.42	0.53	0.25
Rh	-0.20	0.28	0.42	-0.44	-0.68	-0.67	-0.20	-0.23	-0.14	-0.08
Ir	-0.13	0.41	0.58	-0.51	-0.80	-0.78	-0.27	-0.32	-0.23	-0.13
Li				0.55	0.75	0.71	0.51	0.71	0.73	0.38
Na				1.04	1.35	1.30	1.01	1.35	1.41	0.89
K				1.27	1.69	1.64	1.19	1.63	1.69	1.06
V	0.55	1.04	1.27		-0.02	-0.02	-0.03	0.00	-0.01	-0.11
Nb	0.75	1.35	1.69	-0.02		0.00	-0.11	-0.09	-0.13	-0.23
Ta	0.71	1.30	1.64	-0.02	0.00		-0.10	-0.07	-0.11	-0.22
Cr	0.51	1.01	1.19	-0.03	-0.11	-0.10		0.01	0.01	-0.02
Mo	0.71	1.35	1.63	0.00	-0.09	-0.07	0.01		0.00	-0.03
W	0.73	1.41	1.69	-0.01	-0.13	-0.11	0.01	0.00		0.00
Fe	0.38	0.89	1.06	-0.11	-0.23	-0.22	-0.02	-0.03	0.00	
C				-0.50	-0.70	-0.70	-0.23	-0.18	-0.19	0.08
Si				-0.47	-0.52	-0.44	-0.27	-0.49	-0.23	-0.39
Ge				-0.33	-0.42	-0.44	-0.13	-0.07	0.01	-0.09
H	-0.47	-0.30	-0.33	<u>-0.15</u>	<u>-0.16</u>	<u>-0.17</u>	<u>0.25</u>	<u>0.27</u>	<u>0.11</u>	<u>0.15</u>
N	-0.67			<u>-1.10</u>	<u>-1.15</u>	<u>-1.25</u>	<u>-0.60</u>	<u>-0.26</u>	<u>-0.15</u>	<u>-0.03</u>
O	-1.60	-1.30	-1.13	-2.15	-2.10	-3.59	-2.35	-2.21	-2.21	-1.30

(1) The modified embedded-atom method has been extended and successfully applied to a large number of elements encompassing various bonding characteristics. It is found that this simple model can describe the elastic behavior and simple defect properties of these diverse materials.

(2) In this comprehensive study, bulk structural and surface properties have been calculated and compared to experiment and higher level calculations. The surface properties are in reasonable agreement with experiment while the energetics of the bcc metals in open structures is in contradiction with LDA calculations.

(3) An empirical approximation for the background electron density has been developed which includes s -, p -, d -, and f -type angular contributions.

(4) A detailed description of the method of parameter determination has been given and the uniqueness and sensitivity of these parameters to the input data has been addressed. It is stressed that the functions presented here are an attempt at using the model which has not been completely optimized.

(5) It has been found that, in contrast to previous methods, it is sufficient to consider only first-nearest neighbors even in the case of hcp or bcc structures. Energy differences such as the fcc (but not diamond cubic) stacking fault occur naturally from the angular depen-

TABLE IX. Literature values of calculated or experimental heats of formation (eV/atom) Δ_{ij} for equiatomic compounds of diamond cubic and gaseous elements with other elements. No entry indicates that data were not available.

	C	Si	Ge	H	N	O
Cu				-0.10	0.25	-0.78
Ag				-0.37		-0.12
Au				-1.06		
Ni	0.21	-0.45	-0.20		0.36	-0.12
Pd	0.32	-0.57	-0.51	-0.20	0.48	0.00
Pt	0.34	-0.56	-0.43		0.62	
Al	-0.32				-1.60	-3.50
Pb						-1.10
Rh	0.27	-0.44	-0.31		0.46	-0.79
Ir	0.32	-0.40	-0.23		0.59	-0.90
Li				-0.47	-0.67	-1.60
Na				-0.30		-1.30
K				-0.33		-1.13
V	-0.50	-0.47	-0.33		-1.10	-2.15
Nb	-0.70	-0.52	-0.42	-0.20	-1.15	-2.10
Ta	-0.70	-0.44	-0.44		-1.25	-3.59
Cr	-0.23	-0.27	-0.13	-0.08	-0.60	-2.35
Mo	-0.18	-0.49	-0.07		-0.26	-2.21
W	-0.19	-0.23	0.01		-0.15	-2.21
Fe	0.08	-0.39	-0.09	0.15	-0.03	-1.30
C						-0.55
Si				-0.54	-1.09	-3.41
Ge				-0.08	-0.09	-2.18
H		-0.54	-0.08		-0.17	-0.48
N		-1.09	-0.09			
O	-0.55	-3.41	-2.18			

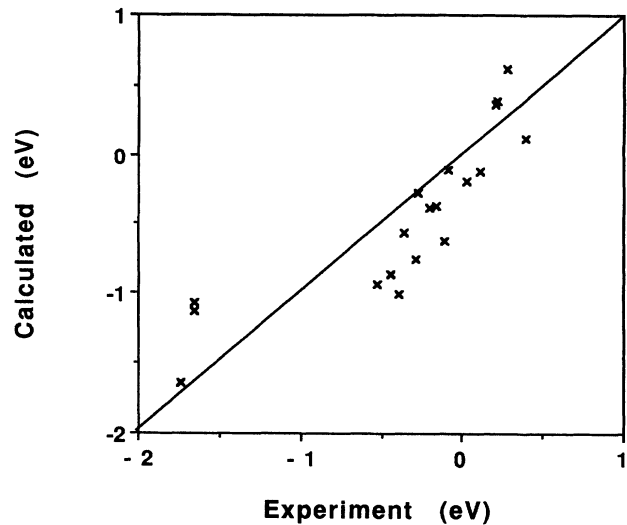


FIG. 4. Calculated vs experimental (Ref. 60) dilute heats of solution (eV) for substitutional solutes in fcc hosts.

dence rather than from long-range interactions.

(6) An environmentally dependent, physically intuitive, screening procedure has been developed. The results of this manuscript are insensitive to the details of the screening procedure.

(7) The formalism of applying the MEAM to alloy systems has been developed and applied to the calculation of dilute heats of solution. A number of severe approximations have been made in these calculations and it is inadvisable to use the alloy potentials until they are fully optimized. Clearly more work needs to be done in this area.

ACKNOWLEDGMENTS

The author would like to thank Dr. R. A. Johnson for his helpful discussions about screening and Dr. C. F. Melius for his careful reading of the manuscript. This work was supported by the U. S. Department of Energy, Office of Basic Energy Sciences, Division of Materials Sciences.

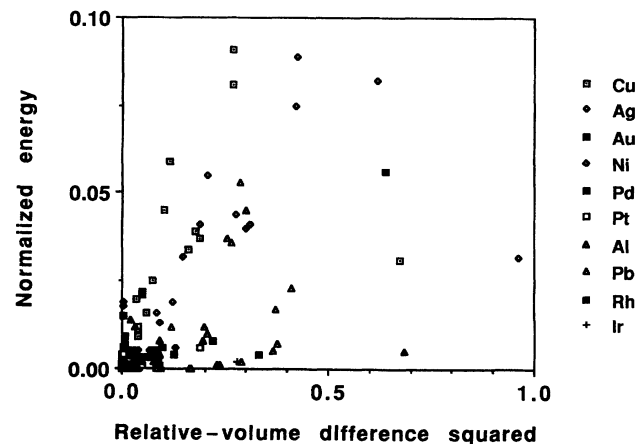


FIG. 5. Scaled relaxation energy vs the square of the relative volume difference for substitutional solutes in fcc hosts.

TABLE X. Calculated dilute heats of solution (eV) for elements in fcc materials. The impurity is substitutional (first-neighbor relaxation included for fcc and bcc but not for diamond cubic impurities) for the solid elements and interstitial (unrelaxed) for the gaseous elements. The second entry, when present, is the experimental value (Ref. 60). Underlined values are taken from experiment (Ref. 59).

	Host									
	Cu	Ag	Au	Ni	Pd	Pt	Al	Pb	Rh	Ir
Cu				-0.12	-1.01	-1.21			-0.72	-0.64
				0.11	-0.39					
Ag				1.20	-0.63	-0.34			0.53	0.78
					-0.11					
Au				0.62	-0.39	-0.17			0.37	0.57
				0.28	-0.20					
Ni	-0.20	0.81	0.39		-0.11	-0.50	-1.64	1.01	-0.35	-0.25
	0.03		0.22		-0.09		-1.74			
Pd	-0.86	-0.76	-0.56	0.04		0.53	-3.06	-1.26	-0.34	-0.26
	-0.44	-0.29	-0.36							
Pt	-0.94	-0.44	-0.36	-0.28	-0.51		-2.99	-0.31	-0.54	-0.52
	-0.53			-0.28						
Al				-1.13	-2.98	-2.97			-2.14	-2.07
				-1.65						
Pb				2.10	-0.14	-1.46			4.79	9.42
Rh	-0.74	0.35	0.24	-0.55	-0.35	-0.50	-2.14	1.05		-0.61
Ir	-0.73	0.55	0.38	-0.68	-0.26	-0.49	-2.09	1.71	-0.72	
Li				0.85	-1.78	-1.47			-0.28	-0.11
Na				5.89	2.56	3.67			5.74	7.26
K										
V	0.51	1.03	-0.72	-0.25	-1.44	-2.11	-1.09	1.12	-1.24	-1.62
Nb	0.80	1.17	-1.17	-0.06	-2.04	-2.65	-0.79	1.48	-1.14	-1.57
Ta	0.73	1.09	-1.05	-0.06	-2.03	-2.62	-0.81	1.71	-1.14	-1.56
Cr	0.56	1.32	0.04	-0.23	-0.66	-1.33	-0.98	1.41	-0.89	-1.23
Mo	1.25	1.99	0.44	0.52	-0.39	-1.11	-0.35	2.64	-0.27	-0.67
W	1.45	2.44	0.97	0.76	0.08	-0.59	-0.01	3.57	0.14	-0.24
Fe	0.46	1.36	0.37	-0.12	-0.24	-0.86	-1.07	1.49	-0.60	-0.85
			0.21				-1.65			
C				-0.05	5.79	4.09	3.36		4.45	4.39
Si				1.49	0.43	-0.53			0.96	0.69
Ge				3.94	0.74	0.21			1.76	1.67
H	<u>0.57</u>	<u>0.59</u>	<u>0.29</u>	<u>0.17</u>	<u>-0.10</u>				<u>0.28</u>	<u>0.77</u>
N	0.50			0.72	0.96	1.24	-3.20		0.92	1.18
O	-1.55	-0.23		-2.40	-1.12		-7.00	-2.20	-1.58	-1.80

APPENDIX

It is appropriate at this point to justify to some extent the physical reasons that interactions of other than first-nearest neighbors may be ignored. It would seem clear that, for the fcc structure where the ratio of second- to first-neighbor distances is 1.4, the exponential decay of electron density can make the second-neighbor contribution to the energy (and elastic constants) small. In fact, this assumption is frequently used in both pair potential and many-body calculations. However, in practice, this natural decay is not rapid enough and the potentials must be artificially terminated to eliminate second-neighbor interactions. The situation in bcc materials is even more ambiguous where the ratio of second- to first-neighbor distances is 1.15. All calculations of bcc materials to date have used at least second-nearest-neighbor interactions. The reality fortunately seems to be that the interaction

between atoms depends upon more than distance. Fu *et al.*⁶¹ have recently shown in density-functional calculations that, at a (100) surface in (bcc) W, the large amount of local screening manifests itself in the fact that only interactions between adjacent layers are important in determining atomic relaxation. That is, the second-nearest neighbors do not play a part even in the bcc structure. This surprising result gives some support to the procedure we have used here in ignoring all but first-neighbor interactions.

Since we have chosen to consider only first-neighbor interactions, it is necessary to provide a cutoff or screening procedure that defines what a nearest neighbor is. This procedure must be continuous in the energy and its first two derivatives to insure that, e.g., spurious minima do not appear in the potential-energy surface or energy is not conserved in a molecular-dynamics calculation due to force discontinuities. It is also desirable that this pro-

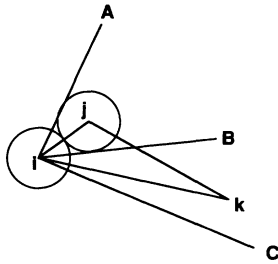


FIG. 6. Schematic of screening of atom k and atom i by atom j . Complete screening occurs if atom k lies within the 60° angle $\angle AiB$. No screening occurs if angle $\angle jik > 60^\circ$.

cedure be computationally simple so as not to dominate the energy calculations. Two basic schemes are typically used to limit the range of interactions. In the first method all distance-dependent functions are smoothly forced to zero at a predetermined (cutoff) distance. This method may be implemented by multiplying the function in question by a "cutoff function" that smoothly goes from the unity to zero as a function of increasing distance^{23,24} or by modifying the function in question by attaching a piecewise continuous "tail" near the end of range.⁶² This method considers atoms only pairwise. A second scheme has been implemented by a number of authors.^{29,63} This method imposes "screening" between an atom and its neighbors by reducing the interaction of any atoms that are not nearest neighbors.

We propose here a "screening" method that takes into account the actual geometry of the atoms under consideration. In Fig. 6, we consider the screening between atoms i and k by atom j . By considering atoms i and j as nearest neighbors with touching atomic spheres, it is easily seen that if atom k lies within the screened cone denoted by angle AiB , it may be considered as completely screened from atom i . Similarly if $\angle jik > 2\angle Bik = 60^\circ$ atom k may be considered as completely unscreened by atom j . For $30^\circ < \angle jik < 60^\circ$, atom k is partially screened and the amount of screening depends upon the distances between the atoms as well as the angle. Thus, we can define a screening function S_{ik} :

$$S_{ik} = \prod_{j (\neq i, k)} S_{ijk}, \quad (\text{A1})$$

where

$$S_{ijk} = \begin{cases} 0, & \theta \leq \pi/6, \\ e^{-As^2(R_{ik}/R_{ij})^{-1}}, & \pi/6 < \theta < \pi/3, \\ 1, & \theta \geq \pi/3, \end{cases} \quad (\text{A2})$$

and $s = \sin(\pi/3 - \theta) / \sin(\theta - \pi/6)$, $\theta = \angle jik$. This ratio s is equal to the ratio of the distances from atom k to iC and

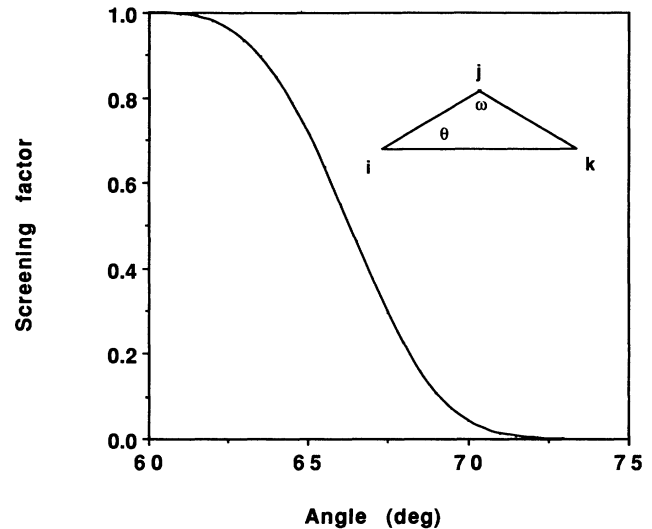


FIG. 7. Screening factor for atoms i and k vs apex angle ω in an isosceles triangle geometry, $ij = jk$.

iB . It is chosen to make S_{ijk} and its first two derivatives continuous. The atom indices for each triad are defined by the condition $R_{jk} \geq R_{ij}$ and $R_{ik} \geq R_{ij}$.

The specific form for S_{ijk} is chosen so that, for close-packed structures, the second derivative of the energy with respect to small vibrational motion of the first neighbors is unaffected. It is certainly not unique. If the constant A is set equal to 500, the contributions from second neighbors are small enough so that the calculated cohesive energy and elastic constants of the bcc structure are essentially the same as when only nearest neighbors are considered.

As an example in Fig. 7, we show the screening factor for atoms i and k in an isosceles triangle with apex angle ω . Note that the screening rapidly increases as ω increases from an equilateral triangle. The base angle used above in Eq. (A2) $\theta = (\pi - \omega) / 2$.

Since the screening is caused by the existence of the electron density of an atom, it should also depend upon the electron density of atom j . A simple possibility (not implemented here) is to multiply the exponent in Eq. (A2) by $\rho_j^{a(0)}(R_{ij})$ and $\rho_j^{a(0)}(R_{jk})$.

The choice of the above screening procedure means that atoms in planar-type structures, e.g., hcp or graphite, naturally interact with more distant out-of-plane atoms even if in-plane atoms are much nearer. Similarly, atoms approaching a free surface will interact with the surface atoms even at distances much greater than the in-plane nearest-neighbor distance. The interactions in these cases are governed by the falloff in electron density rather than by an arbitrary cutoff distance.

¹A. E. Carlsson, in *Solid State Physics: Advances in Research and Applications*, edited by H. Ehrenreich and D. Turnbull (Academic, Boston, 1990), Vol. 43.

²*Atomic Scale Calculations in Materials Science*, MRS Symposia Proceedings No. 141, edited by J. Tersoff, David Vanderbilt,

and V. Vitek (Materials Research Society, Boston, 1988).

³*Atomistic Simulation of Materials*, edited by V. Vitek and D. Srolovitz (Plenum, New York, 1989).

⁴M. S. Daw and M. I. Baskes, *Phys. Rev. Lett.* **50**, 1285 (1983).

⁵M. S. Daw and M. I. Baskes, *Phys. Rev. B* **29**, 6443 (1984).

- ⁶R. A. Johnson and D. J. Oh, *J. Mater. Res.* **4**, 1195 (1989).
- ⁷J. B. Adams and S. M. Foiles, *Phys. Rev. B* **41**, 3316 (1990).
- ⁸M. I. Baskes, S. M. Foiles, and M. S. Daw, *J Phys. (Paris) Colloq.* **49**, C5-483 (1988).
- ⁹M. I. Baskes, M. S. Daw, and S. M. Foiles, in *Atomic Scale Calculations in Materials Science* (Ref. 2), p. 31.
- ¹⁰M. S. Daw and S. M. Foiles, in *1st International Conference on the Structure of Surfaces*, edited by M. A. Van Hove and S. Y. Tong, *The Structure of Surfaces*, Vol. 2 (Springer-Verlag, Berlin, 1984).
- ¹¹M. S. Daw, in *Atomistic Simulation of Materials*, edited by V. Vitek and D. Srolovitz (Plenum, New York, 1988), p. 181.
- ¹²M. S. Daw, *Phys. Rev. B* **39**, 7441 (1989).
- ¹³S. M. Foiles, M. I. Baskes, and M. S. Daw, in *Proceedings of US-Japan Seminar on Electronic Structure and Lattice Defects in Alloys*, edited by R. W. Seigel and F. E. Fujita (Trans Tech, Switzerland, 1987).
- ¹⁴S. M. Foiles, M. I. Baskes, and M. S. Daw, in *Interfacial Structure, Properties and Design*, MRS Symposia Proceedings No. 122, edited by M. H. Yoo, W. A. T. Clark, and C. L. Briant (Materials Research Society, Pittsburgh, 1988), p. 343.
- ¹⁵S. M. Foiles, in *Surface Segregation and Related Phenomena*, edited by P. A. Dowben and A. Miller (CRC, Boca Raton, 1990), Vol. 1, p. 79.
- ¹⁶M. W. Finnis and J. E. Sinclair, *Philos. Mag. A* **50**, 45 (1984).
- ¹⁷V. Rosato, M. Guillope, and B. Legrand, *Philos. Mag. A* **59**, 321 (1989).
- ¹⁸R. A. Johnson, *Phys. Rev. B* **37**, 3924 (1988).
- ¹⁹John R. Smith and Amitava Banerjea, *Phys. Rev. Lett.* **59**, 2451 (1987).
- ²⁰F. Ercolessi, E. Tosatti, and M. Parrinello, *Surf. Sci.* **177**, 314 (1986).
- ²¹M. I. Baskes, *Phys. Rev. Lett.* **59**, 2666 (1987).
- ²²Donald W. Brenner, in *Atomic Scale Calculations in Materials Science* (Ref. 2), p. 59.
- ²³J. Tersoff, *Phys. Rev. Lett.* **56**, 6991 (1988).
- ²⁴M. I. Baskes, J. S. Nelson, and A. F. Wright, *Phys. Rev. B* **40**, 6085 (1989).
- ²⁵A. Antonelli and J. Bernholc, *Phys. Rev. B* **40**, 10 643 (1989).
- ²⁶E. J. Savino, S. Rao, and R. Pasianot, in *Atomic Scale Calculations in Materials Science* (Ref. 2), p. 43.
- ²⁷S. M. Foiles, M. I. Baskes, and M. S. Daw, *Phys. Rev. B* **33**, 7983 (1986).
- ²⁸A. F. Voter and S. P. Chen, in *Characterization of Defects in Materials*, MRS Symposia Proceedings No. 82, edited by R. W. Siegal, J. R. Weertman, and R. Sinclair (Materials Research Society, Pittsburgh, 1987), p. 175.
- ²⁹J. R. Smith and A. Banerjea, *Phys. Rev. Lett.* **59**, 2451 (1987).
- ³⁰J. H. Rose, J. R. Smith, F. Guinea, and J. Ferrante, *Phys. Rev. B* **29**, 2963 (1984).
- ³¹*Metal Reference Book*, edited by C. J. Smith (Butterworths, London, 1976).
- ³²C. S. Barrett and T. B. Massalski, *Structure of Metals* (McGraw-Hills, New York, 1966).
- ³³*Smithells Metals Reference Book*, edited by E. A. Brandes (Butterworths, London, 1983).
- ³⁴K. P. Huber and G. Herzberg, *Molecular Spectra and Molecular Structure IV Constants of Diatomic Molecules* (Van Nostrand-Reinhold, New York, 1979).
- ³⁵N. Saunders, A. P. Miodownik, and A. T. Dinsdale, *CALPHAD* **12**, 351 (1988).
- ³⁶G. Herzberg, *Molecular Spectra and Molecular Structure* (Van Nostrand, Princeton, NJ, 1966).
- ³⁷P. Siegbahn and B. Liu, *J. Chem. Phys.* **68**, 2457 (1978).
- ³⁸P. J. Hay and T. H. Dunning, Jr., *J. Chem. Phys.* **67**, 2290 (1977).
- ³⁹J. N. Murrell, K. S. Sorbie, and A. J. C. Varandas, *Mol. Phys.* **32**, 1359 (1976).
- ⁴⁰A. Banerjea and J. R. Smith, *Phys. Rev. B* **37**, 6632 (1988).
- ⁴¹G. A. Baraff and M. Schluter, *Phys. Rev. B* **30**, 3460 (1984).
- ⁴²J. A. Applebaum and D. R. Hamann, *Surf. Sci.* **74**, 21 (1978).
- ⁴³M. I. Baskes and C. F. Melius, *Phys. Rev. B* **20**, 3197 (1979).
- ⁴⁴R. W. Balluffi, *J. Nucl. Mater.* **69 & 70**, 240 (1978).
- ⁴⁵W. Wycisk and M. Feller-Kniepmeier, *J. Nucl. Mater.* **69 & 70**, 616 (1978).
- ⁴⁶*Vacancies and Interstitials in Metals*, edited by A. Seeger, D. Schumacher, W. Schilling, and J. Diehl (North-Holland, Amsterdam, 1970).
- ⁴⁷*Vacancies and Interstitials in Metals and Alloys*, edited by C. Abromeit, and H. Wollenberger (Trans. Tech, Switzerland, 1987).
- ⁴⁸*Point Defects and Defect Interactions in Metals*, edited by Jin-ichi Takamura, Masao Doyama, and Michio Kiritani (North-Holland, Amsterdam, 1982).
- ⁴⁹J. Bernholc, A. Antonelli, T. M. Del Sole, Y. Bar-Yam, and S. T. Pantelides, *Phys. Rev. Lett.* **61**, 2689 (1988).
- ⁵⁰H. d'Amour, W. Denner, H. Schulz, and M. Caradona, *J. Appl. Crystallogr.* **15**, 148 (1982).
- ⁵¹C. S. G. Cousins, L. Gerward, J. Staun Olsen, B. Selsma, and B. J. Sheldon, *J. Appl. Crystallogr.* **15**, 154 (1982).
- ⁵²G. J. Ackland and M. W. Finnis, *Philos. Mag. A* **54**, 301 (1986).
- ⁵³W. R. Tyson and W. A. Miller, *Surf. Sci.* **62**, 267 (1977).
- ⁵⁴B. Hyland (private communication).
- ⁵⁵C. L. Fu, S. Ohnishi, H. J. F. Jansen, and A. J. Freeman, *Phys. Rev. B* **31**, 1168 (1985).
- ⁵⁶A. T. Paxton, M. Methfessel, and H. M. Polatoglou, *Phys. Rev. B* **41**, 8127 (1990).
- ⁵⁷F. R. de Boer, R. Boom, W. C. M. Mattens, A. R. Miedema, and A. K. Niessen, in *Cohesion and Structure*, edited by F. R. de Boer and D. G. Pettifor (North-Holland, Amsterdam, 1988), Vol. 1.
- ⁵⁸*Handbook of Binary Metallic Systems-Structure and Properties* (NTIS Israel Program for Scientific Translations, Jerusalem, 1967), Vol. II, translated from Russian.
- ⁵⁹R. B. McLellan and C. G. Harkins, *Mater. Sci. Eng.* **18**, 5 (1975).
- ⁶⁰R. Hultgren, P. D. Desai, D. T. Hawkins, M. Gleiser, and K. K. Kelley, *Selected Values of the Thermodynamic Properties of Binary Alloys* (American Society for Metals, Metals Park, OH, 1973).
- ⁶¹C. L. Fu, S. Ohnishi, E. Wimmer, and A. J. Freeman, *Phys. Rev. Lett.* **53**, 675 (1984).
- ⁶²R. A. Johnson, *J. Phys. F* **3**, 293 (1973).
- ⁶³K. E. Khor and S. Das Sarma, *Phys. Rev. B* **38**, 3318 (1988).